Influence of building collapse on pluvial and fluvial flood inundation of metro stations in central Shanghai

Zhi Li[1], Hanqi Li[1], Zhibo Zhang[1], Chaomeng Dai[1], and Simin Jiang[1]

[1]College of Civil Engineering, Tongji University, Shanghai, China

Correspondence: Zhi Li (zli90@tongji.edu.cn)

Abstract. Urban flooding poses a significant threat to vulnerable underground infrastructure systems, such as metro stations. Building collapses induced by earthquakes alters urban building layout and coverage, consequently influencing flood inundation and propagation patterns. This study employs GPU-accelerated hydrodynamic simulation to investigate the mechanisms by which building collapse affects subsequent pluvial or fluvial flooding in the Huangpu district of Shanghai. Massive building
5 collapse layouts are randomly generated, on which hydrodynamic simulations are performed and the inundation process of the metro stations are analyzed. The results reveal that pluvial floods are strongly influenced by localized topography distributed across the city. Consequently, building collapse has a more substantial impact on pluvial flooding when more buildings are collapsed. In contrast, fluvial floods are sensitive to the source location (e.g., location of levee breach) and the long travel route. Building collapse can either positively or negatively influence fluvial flooding by constricting or blocking the flow path. This
10 work highlights the complex mechanism of earthquake-flood multi-hazard processes, emphasizing the importance of performing local-to-local analysis when both the hazard (e.g., individual building collapse, fluvial flood) and the hazard-bearing body (e.g., metro station) are localized. To better serve urban disaster prevention and mitigation, more efforts should be directed on developing physics-based high-resolution urban earthquake-flood simulation methods, as well as on acquiring data to drive such simulations.

1 Introduction

15 Climate change and urbanization have increased human exposure to urban flood hazards, particularly in the East Asia (Cao et al., 2022; Rentschler et al., 2023). To enhance urban resilience to flood hazards, there is an urgent need to understand the physical processes of flood propagation under various current and future scenarios. Hydrodynamic modeling is an important tool for urban flood studies. Recent advancements in high-performance parallel computing (HPC) have facilitated
20 city-scale, high-resolution (on $< 5m$ resolution digital elevation model, DEM) rapid hydrodynamic simulations (Guo et al., 2021; Morales-Hernández et al., 2021; Sanders and Schubert, 2019; Schubert et al., 2022a). Combining HPC technology and traditional hydrodynamic models, the high resolution spatial-temporal evolution of the inundation depth and extent can be reproduced or predicted, thereby aiding in the design and improvement of flood mitigation strategies.

When considering urban flood resilience, metro systems are the weak link. Underground infrastructures are inherently more
25 vulnerable to floods, and evacuating passengers from inundated metro tunnels poses immense challenges. Megacities typically

have well-developed metro systems, but flooding of the urban metro system has been reported worldwide (Aoki et al., 2016; Forero-Ortiz et al., 2020; Toda et al., 2009). In China, megacities including Beijing, Shanghai, Guangzhou, Wuhan and Shenzhen have more or less experienced flooding of their metro lines (Lyu et al., 2019, 2020; Wang et al., 2021). In July 2021, a tunnel of the Zhengzhou (China) metro Line 5 was inundated due to heavy rainfall and inadequate emergency response measures, resulting in 14 fatalities (Yang et al., 2022). This devastating incident has raised nationwide concerns regarding comprehensive flood risk evaluation and the urgent need for robust mitigation strategies tailored specifically for urban metro systems.

Modern metro stations and tunnels feature multiple flood prevention equipment such as flood gates, sand bags and pumps. The entrance of the metro stations are often elevated to avoid flooding. These flood prevention measures are expected to work well under most circumstances. However, it remains unclear if these measures are fully functional under extreme multi-hazard scenarios. Multi-hazard refers to scenarios where a system or infrastructure (e.g., a metro station) is subjected to multiple hazardous events, either concurrently or sequentially. The compounding effects of multi-hazards can potentially lead to more severe consequences compared to the impact of individual hazards. Compound flood is a common multi-hazard scenario. In 2013, typhoon Fitow triggered heavy rainstorm in Shanghai, China. At the same time, fluvial flood from the upstream attacked Shanghai. An astronomical high tide further exacerbated the compound flood, which finally caused 2 deaths and a loss of approximately 150 million US dollars. Geological hazards also compound the impacts of urban floods (Gill and Malamud, 2014). For example, it has been shown that land subsidence exacerbates flood depth and extent (Johnston et al., 2021; Navarro-Hernandez et al., 2023). Another example is the sequential occurrence of a magnitude 7.8 earthquake in April 2015 and a severe flood event in August 2017 within the same region of central Nepal. The infrastructure damaged during the seismic event had not been fully rehabilitated when the flooding occurred, leading to more devastating damage compared to if the area was attacked by a single disaster (Gautam and Dong, 2018). For coastal cities, earthquake could induce tsunami, which turns into coastal floods. After the earthquake, the flood resilience could be compromised due to two main factors: (i) the flood-prevention structures (e.g., flood walls) and equipment (e.g., pumps) could be damaged during the earthquake, and (ii) the collapsed buildings could block the evacuation routes. The confluence of these two factors can exacerbate the severity of coastal flooding impacts (Goda et al., 2019; Ito et al., 2020; Román-de La Sancha et al., 2022; Takabatake et al., 2022).

Urban multi-hazard studies have attracted increasing attentions in recent years. However, existing studies often focus on risk assessment that is based on historical data or simplified simulations (e.g., Depietri et al., 2018; Owolabi and Sajjad, 2023). With the advances in HPC and urban flood simulation, it is possible to reproduce large-scale, high-resolution flood propagation process under multi-hazard scenarios. This allows for an investigation on the physical mechanisms how multi-hazards affect urban flooding compared with pluvial or fluvial flood hazard alone. With better depiction of the multi-hazard flooding process, risk assessment methodologies can be enhanced too. However, an in-depth exploration of improved risk assessment techniques is beyond the scope of the present manuscript.

In this work, we use high-resolution hydrodynamic simulations to estimate the evolution of pluvial/fluvial flood depth at 17 metro stations in the Huangpu district located in the central region of Shanghai. We compare the flooding dynamics in the actual Huangpu district to scenarios that incorporate multiple random realizations of building collapse. In these simulated

scenarios, certain buildings are assumed to have collapsed, obstructing roads and altering the urban layout. This approach serves as an approximation of post-earthquake conditions, enabling the analysis of the multi-hazard process involving the cascading impacts of seismic activity and subsequent inundation. We aim at understanding if, how and why earthquake-induced building collapse affect the inundation of the metro stations. The findings will serve as the cornerstone for multi-hazard risk assessment

65 of urban metro systems. As depicted in Fig. 1, the primary focus is on quantifying the hydrodynamic consequences of collapsed structures on flood propagation and accumulation at metro stations. Topics such as how the earthquake is triggered, how the buildings are collapsed and how the flood enters the metro station are beyond the scope of this manuscript.
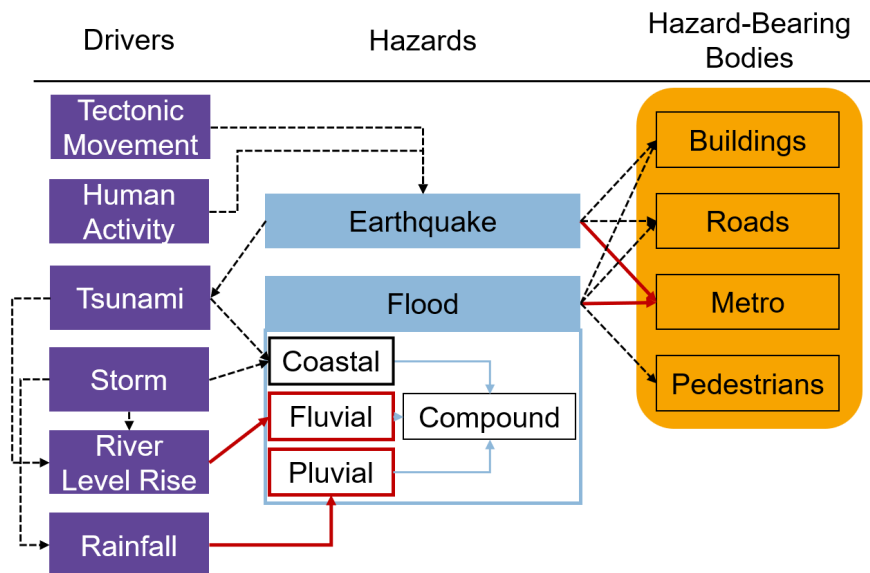
Figure 1. A flowchart of possible earthquake-flood multi-hazard mechanisms. The red lines delineate the focus of this manuscript.

The rest of this manuscript is arranged as follows: Section 2 describes the study site (Section 2.1), the numerical simulation methods (Section 2.2) and the building collapse scenarios (Section 2.3). Section 3 reports and analyzes the simulation results.

70 Section 4 discusses the implications, limitations and future works of this study. Section 5 draws the conclusions.

2 Methods

2.1 Study Area

The study area is the Huangpu district located in the center of Shanghai. Shanghai is one of the largest cities in China, with a population of approximately 25 million. Huangpu district has an area of about 20 square kilometers and a population of 0.66

75 million. Huangpu district is bounded by the Suzhou River in the north and the Huangpu river in the east and south. The west

boundary connects the Jingan and Xuhui districts of Shanghai (Fig. 2). As of 2023, the Shanghai metro system has 19 metro lines, in which 8 lines pass through the Huangpu district, forming 17 stations (labeled as station 1 to 17 in Fig. 2).

Multiple drivers could lead to or aggravate flooding in Shanghai, including typhoon, astronomical high tide, upstream fluvial flood, low-lying topography, sea level rise and land subsidence. These factors make Shanghai one of the most vulnerable cities to flood in the world (Balica et al., 2012). Shanghai adopts four levels of flood defense systems: the sea walls, the river flood walls, the pump stations and the pipe drainage system. The current defense system is generally effective, but might be inadequate under occasional extreme conditions or future climate change scenarios (Ke et al., 2021; Yin et al., 2021; Zhou et al., 2017). For example, Shanghai experienced a short but intense rainfall event on July 21th of 2023, with a maximum rainfall rate exceeding 100mm per hour (Fig. 3), leading to mild waterlog. The reported inundation depth reach 25cm at multiple locations in the city. It remains important to better understand the flooding mechanisms in Shanghai and keep improving flood prevention system and flood response strategies correspondingly.

2.2 Numerical Simulation

In this work, the flooding of the Huangpu district is simulated with the SERGHEI-SWE model (Caviedes-Voullième et al., 2023). SERGHEI-SWE is an open-source, high-performance hydrodynamic model. It solves the two dimensional shallow water equations (SWE) on Cartesian grids using Godunov-type finite-volume methods (Morales-Hernández et al., 2021). SERGHEI-SWE is a parallel SWE solver that achieves performance portability across a variety of computational backends, such as OpenMP, CUDA and HIP. This feature is achieved through the Kokkos framework (Trott et al., 2022). It also supports distributed memory parallelization through MPI. GPU computing have dramatically reduced the computational cost for large-scale hydrodynamic simulations. Caviedes-Voullième et al. (2023) has shown that using SERGHEI-SWE, for a computational domain with 0.5 million grid cells, hydrodynamic simulations on a workstation GPU remain faster than that on 128 CPU threads. Thus, SERGHEI-SWE with GPU computing capability is an ideal tool for completing massive flood simulation scenarios (e.g., the multiple random building collapse scenarios used in this study) within an acceptable time frame.

To build the hydrodynamic model for the Huangpu district, data on the DEM, surface roughness and boundary conditions are required. Flood simulation results are sensitive to the DEM (Xu et al., 2021). The 30m resolution DEM of the study area is freely available online, but this resolution is too coarse to resolve individual buildings and road sections, which have significant influence on the flood propagation pathways. Thus, the DEM is downscaled onto 5m grids, resulting in 1.36 million grid cells. It should be noted that DEM downscaling does not improve the accuracy of the DEM itself, but allows for better delineations of the building outlines. The building shape and height data are integrated into the DEM, replacing the original coarse-resolution building pixels. The final DEM can be visualized in Fig. 2.

The road layout data is integrated into the land use file, which provides spatially-distributed surface roughness for computing the bottom drag. In this work, the land use of the study area is simplified to three types: buildings, roads and others. They are assigned with a Manning's roughness coefficient of $0.012s/m^{1/3}$, $0.016s/m^{1/3}$ and $0.03s/m^{1/3}$ respectively. Arguably, 5m grid resolution does not resolve the road shoulders. Existing approaches such as the artificial porosity model and the elevated edge model could identify the subgrid-scale road shoulders (e.g. Guinot et al., 2018; Hodges, 2015; Li and Hodges, 2019), but
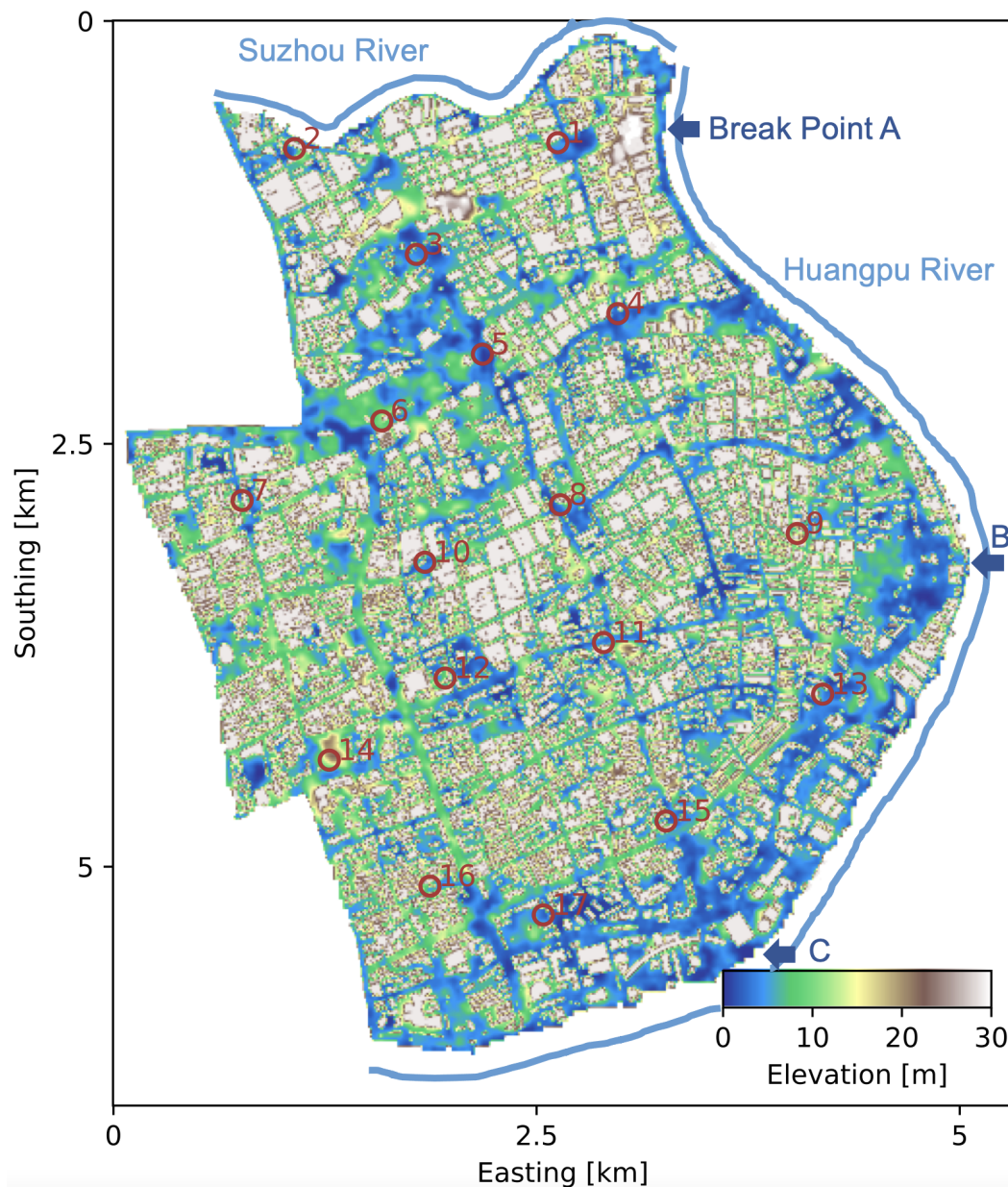
Figure 2. The DEM of the study area. The red markers indicate the 17 metro stations in the study area. The dark blue arrows are the hypothetical break points of the flood wall. For better visualizations, buildings are assigned with a uniform elevation of 29m on this figure, but their original elevation is used in the simulations.

110   they are not adopted herein because the focus of this manuscript is on comparing the pre- and post-collapse scenarios. Indeed, the influence of the road shoulders on flood propagation does not depend on the building collapse status. Building drag force
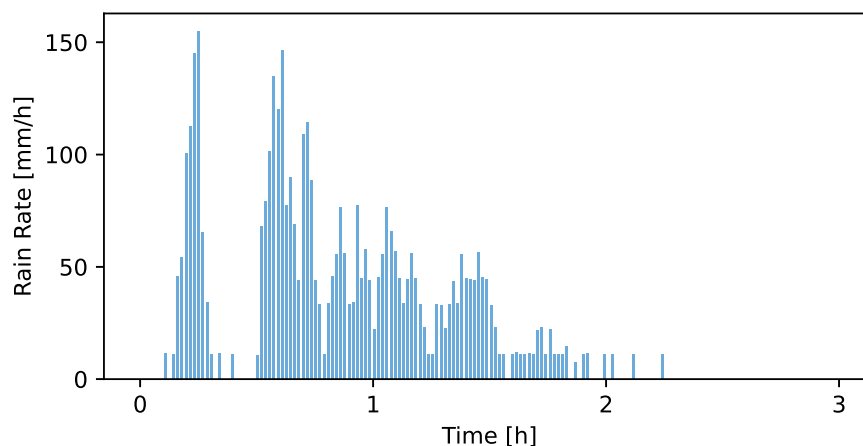
Figure 3. The rainfall data recorded at the Tongji University main campus between 2:30pm and 5:30pm, July 21th of 2023.

is neglected in the simulations. Rainfall is allowed to fall on the building roof, then flow to its neighboring cells following the topographical gradient. Detailed roof storage or drainage devices are not considered due to the lack of data. Soil infiltration and drainage through the stormwater pipelines are both ignored. Admittedly, this would overestimate the flood inundation
115   depth. However, under extreme flood events, the soil and the drainage pipes are likely saturated, meaning that they have minor influence on surface hydrodynamics (e.g., Wilfong et al., 2024). More detailed discussions on the roles of infiltration and drainage can be found in Section 4. The computational domain is initially dry. The west boundary of the domain is open and water is allowed to exit the domain freely. All other boundaries are closed to represent fully functioned flood walls along the rivers.

120   The flood simulations conducted in this study encompass two distinct scenarios: fluvial and pluvial flooding events. To model fluvial flood, assume three locations on the flood wall are breached (e.g., due to earthquake) and a constant water depth of 3m is enforced at the three breakpoints (marked on Fig. 2). To model pluvial flood, assume the rainfall rate equals the recorded precipitation on July 21th of 2023 (Fig. 3). Both scenarios are modeled for 3 hours. The inundation extent, depth, particularly the depth at the 17 metro stations, will be monitored and analyzed.

125   **2.3   Building Collapse Model**

The earthquake risk of Shanghai is generally low. Historically, Shanghai rarely experiences an earthquake with a magnitude greater than VII. However, the large population density, tunnel constructions in the soft soil, massive old civil houses as well as more than 150 skyscrapers (i.e., buildings taller than 150m) make Shanghai vulnerable to potential earthquake attacks. It is estimated that in the Nanjing Road (located in Huangpu district) where plenty of old houses are made of brick and timber, 7.2%
130   of buildings will be seriously damaged under an intensity VI earthquake, and 24.8% of buildings will be seriously damaged under an intensity VII earthquake (Cole et al., 2008).
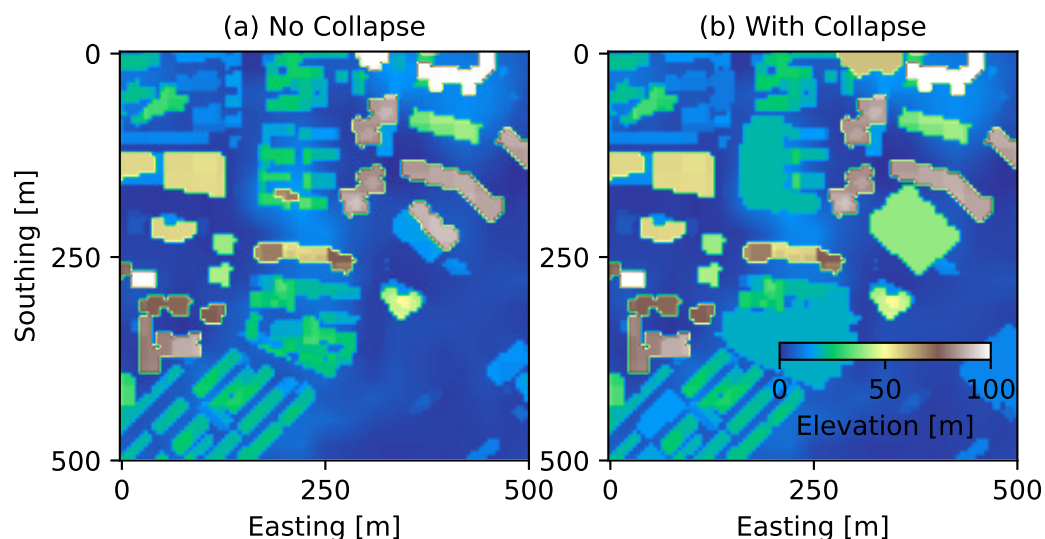
Figure 4. A comparison between (a) the original DEM and (b) the DEM with a few buildings collapsed.

In the present study, earthquake-induced building collapse is not explicitly modeled. Instead, we generate n realizations with $r\%$ randomly selected buildings collapsed. From modeling perspective, this is equivalent to perform hydrodynamic simulations with n different DEM and roughness inputs representing various building damage scenarios. Herein, $n =100$ and $r =10$, 20 or 40 respectively. By analyzing hydrodynamic simulation results from 100 possible building collapse scenarios, the inundation patterns of the metro stations can be statistically characterized. Then, typical building collapse and metro station inundation scenarios will be examined in more detail, revealing deterministic flood propagation mechanisms underlying the statistical observations.

Similar to Takabatake et al. (2022), building collapse is modeled by distributing 50% of the original building volume, estimated from the building footprint area and height data, to its surroundings. This results in shorter structures with a broader spatial occupancy after collapse (Fig. 4). Although it is an idealized representation that neglects factors such as building strength and seismic force magnitude, this approach effectively characterizes the obstruction and alteration of flood propagation paths by collapsed buildings, which is the primary focus of this study. The simplified modeling of post-collapse building geometry captures the essential effects on flood dynamics without introducing unnecessary complexities.

3 Results

Before illustrating the simulation results, it is necessary to define a few quantitative metrics that aid the analysis. Herein, three metrics are defined: the average deviation of water depth (ϵ_{avg}), the percent of flooded scenarios (p_{flooded}), and the percent of the aggravated scenarios (p_{agg}, see Eq. 1-3).

7

$$\epsilon_{\mathrm{avg}} = \frac{\sum_{i=1}^{n} \left[\overline{h_i(t) - h_{\mathrm{ref}}(t)} \right]}{n} \tag{1}$$

$$p_{\mathrm{flooded}} = \frac{n_{\mathrm{flooded}}}{n} \tag{2}$$

$$p_{\mathrm{agg}} = \frac{n_{\mathrm{agg}}}{n_{\mathrm{flooded}}} \tag{3}$$

In Eq. (1)-(3), $h_{\mathrm{ref}}(t)$ is the simulated depth for the reference scenario (i.e., without building collapse) at a given metro station, $h_i(t)$ is the simulated depth of the ith random building collapse scenario, the overbar indicates time averaging over the 3-hour simulation period, $n = 100$ is the total number of testing simulations, n_{flooded} is the total number of testing scenarios in which a given station is flooded (i.e., the maximum water depth exceeds 1cm) and n_{agg} is the number of testing scenarios with greater flood depth than the reference scenario at the given station.
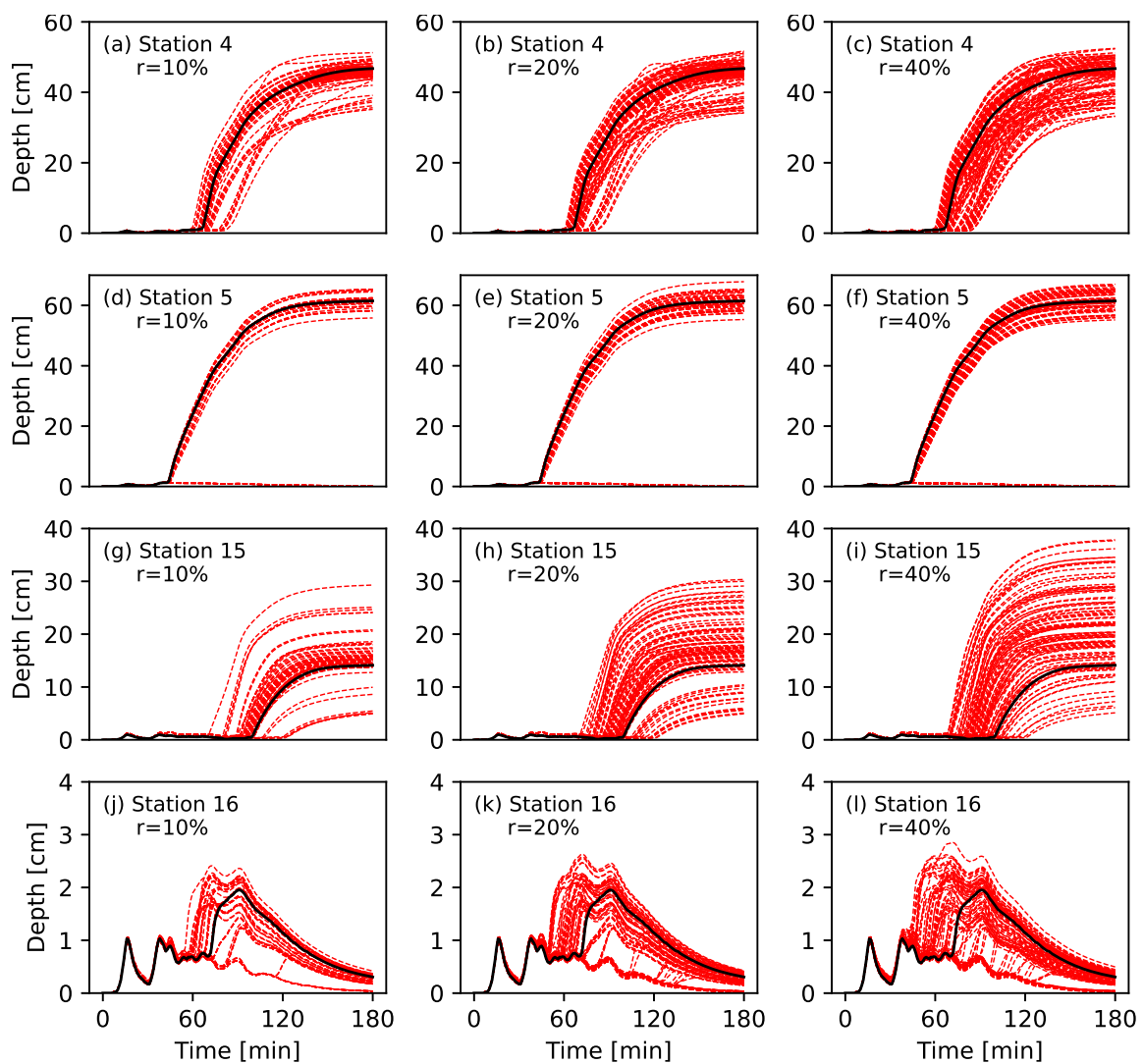
3.1 Pluvial Flood

Figure 5 shows the inundation depth at metro stations 4, 5, 15 and 16 under pluvial flood scenarios. The thick black curve represents the reference scenario without building collapse. The red curves are the 100 random building collapse scenarios. Other stations are either not flooded, or the water is too shallow to cause any catastrophic impact. It can be seen that building collapse has influence on the inundation depth at all four stations displayed. For each station, different building collapse scenarios could either increase or decrease the inundation depth compared with the reference scenario. Station 4, 5 and 15 show similar inundation patterns, where the water depth is small initially, then surges to tens of centimeters. It indicates that these stations are located in low-lying areas that receive water from their surroundings. Station 16 is different in that the water depth declines when rainfall weakens after about 90 minutes, meaning that station 16 both distributes water to its surroundings, and receives water from its surroundings. The latter is evidenced by the different depth evolution patterns with respect to different building collapse scenarios.

Interestingly, Fig. 5 shows that, at station 5, despite most building collapse scenarios exhibit an increasing water depth to about 60cm, a few scenarios are almost not flooded (characterized by the near-zero water depth). Detailed examination (not shown) reveals that station 5 is close to a building. When this building is randomly chosen to collapse, station 5 is completely buries and is unaffected by flood. This situation is not impossible in the real world because there exists metro station entrances inside the buildings in Shanghai. When such buildings collapse to bury the entrance, although flood water is more difficult to invade the station, passengers are more difficult to evacuate too. It implies that for a complete analysis of multi-hazard risk of the metro stations, the locations of each entrance should also be considered separately, but this is beyond the scope of the present study.

As more buildings are collapsed (r increases), the envelopes of the inundation depths expand, implying that more and more building collapse scenarios diverge from the reference scenario. It can be seen from Table 1 that ϵ_{avg} increases with r at all three stations, indicating that the change of building layout (due to building collapse) has strong impact on the flood water propagation. The same conclusion was also mentioned in Bruwier et al. (2020). At all three stations displayed and with all r

Figure 5. Water depth evolution at metro station 4, 5, 15 and 16 for the pluvial flood scenarios. The black line is the original DEM without building collapse. The red lines are the 100 random realizations with buildings collapsed.

180 values tested, 100% of the testing scenarios are flooded. That is, although building collapse affects the magnitude of flooding at metro stations, it does not change the inundation status. This is in contrast to the case of fluvial flood, which will be discussed later in Section 3.2 The p_{agg} values exhibit different behaviors as r increases at the three stations. For station 4, building collapse generally alleviate the flood risk as p_{agg} remains less than 50%. Station 15 shows the opposite behavior (with $p_{agg} \geq 80\%$), where building collapse mostly enhance flood risk. For station 5, p_{agg} decreases from 67% to 26% as r increases. Clearly,

185 it is difficult to evaluate the increased/decreased flood risk from an ensemble point of view, as it is the specific buildings that collapse (which are different for different scenarios) determine the subsequent flood propagation and water accumulation patterns.

Table 1. The mean deviation from the reference scenario, the proportion of scenarios being flooded, and the proportion of scenarios with aggravated flood disaster (i.e., greater depth than the reference) among the 100 random building collapse and pluvial flood scenarios.

	Station 4			Station 5			Station 15		
	$r =10\%$	$r =20\%$	$r =40\%$	$r =10\%$	$r =20\%$	$r =40\%$	$r =10\%$	$r =20\%$	$r =40\%$
ϵ_{avg} [cm]	1.43	2.54	3.42	4.16	9.35	13.6	1.22	2.99	4.95
$p_{flooded}$					100%				
p_{agg}	45%	32%	36%	67%	37%	26%	85%	80%	85%

To further uncover the mechanisms how building collapse affect inundation, three scenarios are selected and analyzed in detail, which are the reference scenario (no building collapse) and the scenarios with the largest and smallest inundation depth

190 (30cm and 5cm respectively) at metro station 15 ($r =20\%$). As can be seen from Fig. 6, with pluvial flood, water accumulates in local topographic depressions, resulting in discrete inundated areas across the study region. In all three scenarios, an inundation patch is present in the vicinity of station 15, posing a potential flood risk to this metro station. However, Fig. 6(d) sees buildings collapsed on the northwest of station 15, leading to less depression area that stores water (comparing Fig. 6c with Fig. 6a) and reduced road width between buildings that enhances flow speed (comparing Fig. 6d with Fig. 6b). Both factors facilitate

195 flood propagation towards station 15. On the contrary, in Fig. 6(f), building collapse occurs away from station 15, which has minor influence on the inundation of station 15 because pluvial flood is strongly affected by the local topography. Clearly, the influence of building collapse on pluvial flood propagation is highly localized. Flooding of a metro station is not expected to aggravate if the buildings near the station do not collapse. This finding also explains why $p_{flooded}$ stays at 100% under all circumstances (Table 1), as the localized influence of building collapse can hardly affect the city-wide occurrence of pluvial

200 flood.

3.2 Fluvial Flood

Figure 7 shows the inundation depth at metro stations 4, 13 and 17 under fluvial flood scenarios. Other stations are either not flooded, or the depth is too small (e.g., less than 1cm). This is expected because the three stations displayed are close to the break points of the flood wall (Fig. 2). Station 4 is not flooded in the reference scenario, and hardly flooded when $r =10\%$
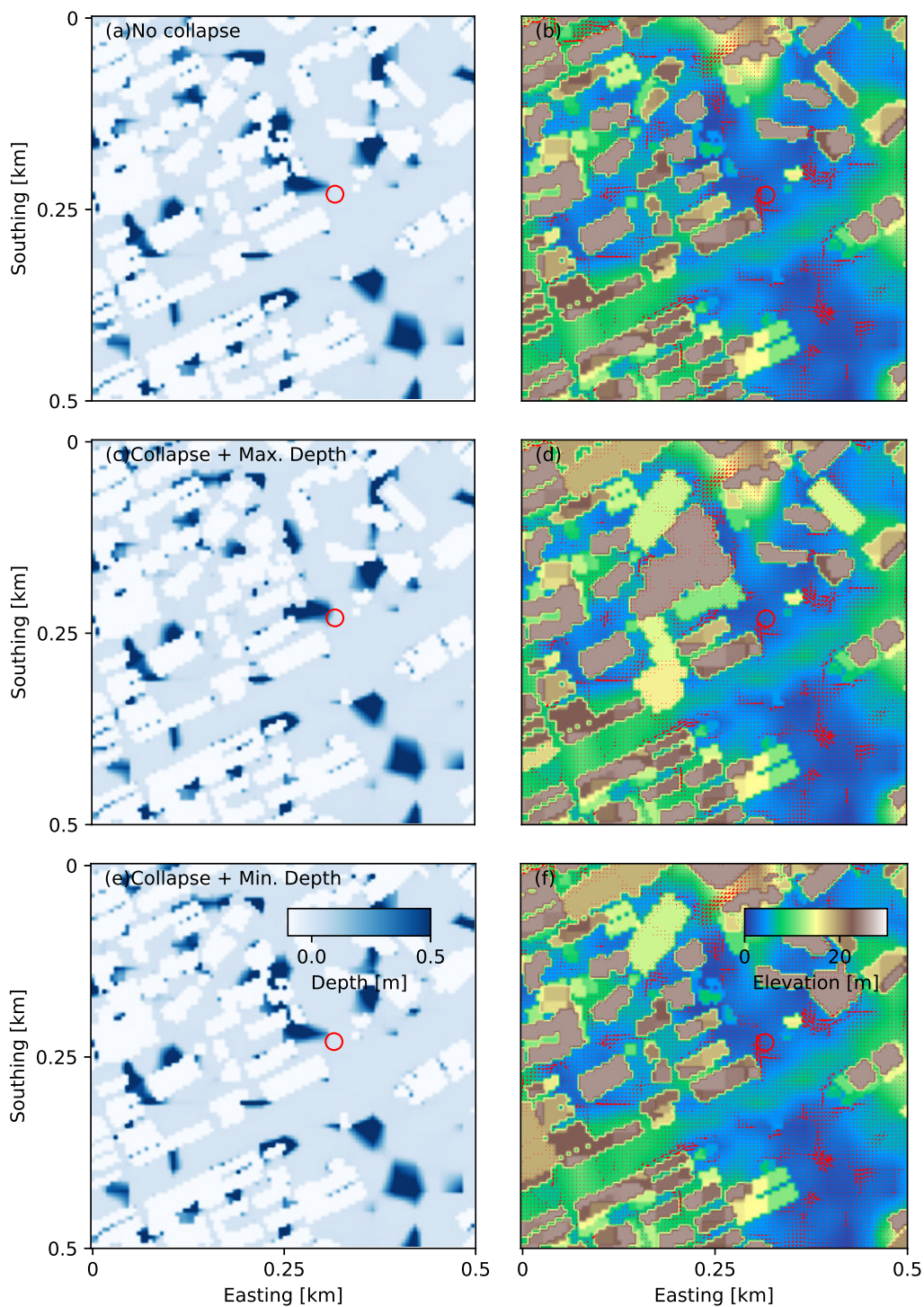
Figure 6. Simulated water depth (left column) and velocity (right column, on top of DEM) at 1 hour for selected pluvial flood scenarios near metro station 15 (r=20%). The top row is the reference scenario without building collapse (the black curve in Fig. 5h). The middle row is associated with the building collapse scenario with the largest inundation depth at station 15, whereas the bottom row represents the scenario with the smallest inundation depth. The red circle is the location of station 15.

205 and 20%. Only a few realizations exhibit non-negligible inundation depth (Fig. 7b). When r is increased to 40%, 17 out of the 100 random realizations are flooded (Table 2). Clearly, building collapse enhances the flood exposure of station 4 and the exposure exacerbate as r increases. Station 13 exhibits the opposite behavior, where a large r reduces flood exposure. At $r =$40% (Fig. 5f), only 28 out of the 100 scenarios show positive flood depth. With $r =$10% and 20%, however, these numbers are 78 and 62 respectively (Table 2). A similar trend is observed at station 17, where a large r reduces flood exposure (only 10

210 scenarios are flooded at $r =$40%).
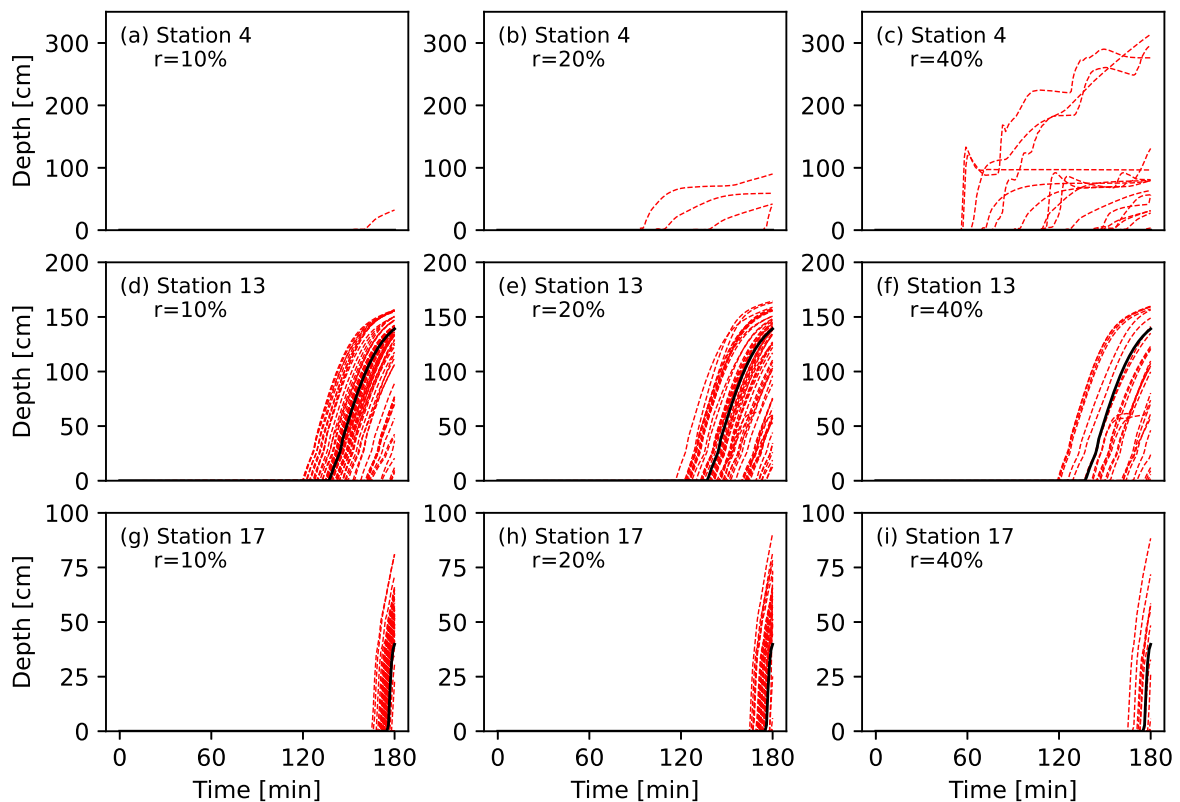
Figure 7. Water depth evolution at metro station 4, 13 and 17 for the fluvial flood scenarios. The black line is the original DEM without building collapse. The red lines are the 100 random realizations with buildings collapsed.

A notable difference between fluvial and pluvial flood is that, unlike pluvial flood scenarios where p_{flooded} always reach 100%, for fluvial flood, both water depth and p_{flooded} exhibit variability between different stations, different r values, and different random realizations (Table 2). In terms of the mean deviation (ϵ_{avg}), the trends of ϵ_{avg} and p_{flooded} are the same for station 4 and 17. With more testing scenarios flooded, the mean deviation increases. However, this trend is reversed at station

215 13, where the lowest p_{flooded} ($p_{\text{flooded}} =$28% at $r =$40%) is accompanied with the largest deviation ($\epsilon_{\text{avg}} =$22.29cm). Again, these results illustrate the complex interactions between flood propagation and the collapsed buildings.

Table 2. The mean deviation from the reference scenario, the proportion of scenarios being flooded, and the proportion of scenarios with aggravated flood disaster (i.e., greater depth than the reference) among the 100 random building collapse and fluvial flood scenarios.

	Station 4			Station 13			Station 17		
	$r=10\%$	$r=20\%$	$r=40\%$	$r=10\%$	$r=20\%$	$r=40\%$	$r=10\%$	$r=20\%$	$r=40\%$
ϵ_{avg} [cm]	2.30	4.32	10.02	13.72	20.02	22.29	2.11	1.60	1.36
p_{flooded}	1%	4%	17%	78%	62%	28%	61%	33%	10%
p_{agg}		100%		46%	37%	22%	92%	88%	70%

Figure 8 shows three selected scenarios to better understand the flooding process of station 13. At the end of the simulation, the water depth at station 13 reaches about 140cm for the reference scenario. As can be seen from Fig. 8(b), the flood water originates from break point B (Fig. 2). The intruding water travel southward following the terrain slope. Then it change direction
220 towards the west when encountering elevated terrains, and turn back to south again when hitting buildings. After penetrating through a few building blocks, the river water finally reach station 13. Figure 8(c) and (d) display the scenario with the deepest water depth at station 13. An obvious distinction is that some buildings along the Huangpu River are collapsed. The collapsed buildings squeeze the roads between them, which serve as a primary path of the intruding water. As a result, the flow velocity is higher and station 13 is flooded with greater depth. Figure 8(e) and (f) show the scenario with the lowest inundation depth
225 at station 13. Although the flow path is squeezed by the collapsed buildings as well, additional buildings are collapsed next to station 13 in the northeast, which blocks the original southward flow path penetrating these buildings. As a result, the flooding of station 13 is weakened and postponed.

4 Discussions

4.1 Pluvial vs. Fluvial

230 From the results shown in Section 3, pluvial and fluvial floods exhibit distinct behaviors in the event of building collapses. Pluvial flood occur in low-lying areas all around the study area. Building collapse do not alter the flood status (p_{flooded} always equal 100%) of a given location (i.e., a metro station), but greater variance of the inundation depth is detected as more buildings collapse. Fluvial flood occur close to the rivers. Its occurrence is sensitive to building collapse. As r increases, the total number of flooded scenarios could either increase (station 4) or decrease (station 13 and 17).

235 The distinctions between pluvial and fluvial floods arise from their different origination, accumulation, and propagation patterns. Pluvial floods originate from heavy rainfall, which is spatially distributed. Rainwater accumulates in local topographic depressions, leading to massive short travel paths, which can be visualized from the velocity field of Fig. 6. Most flow paths remain unaffected by building collapse unless the collapsed building is in close proximity to the depression. As r increases, there is a greater probability that a chosen location is next to the collapsed building, which explains why more scenarios diverge
240 from the reference at higher r.
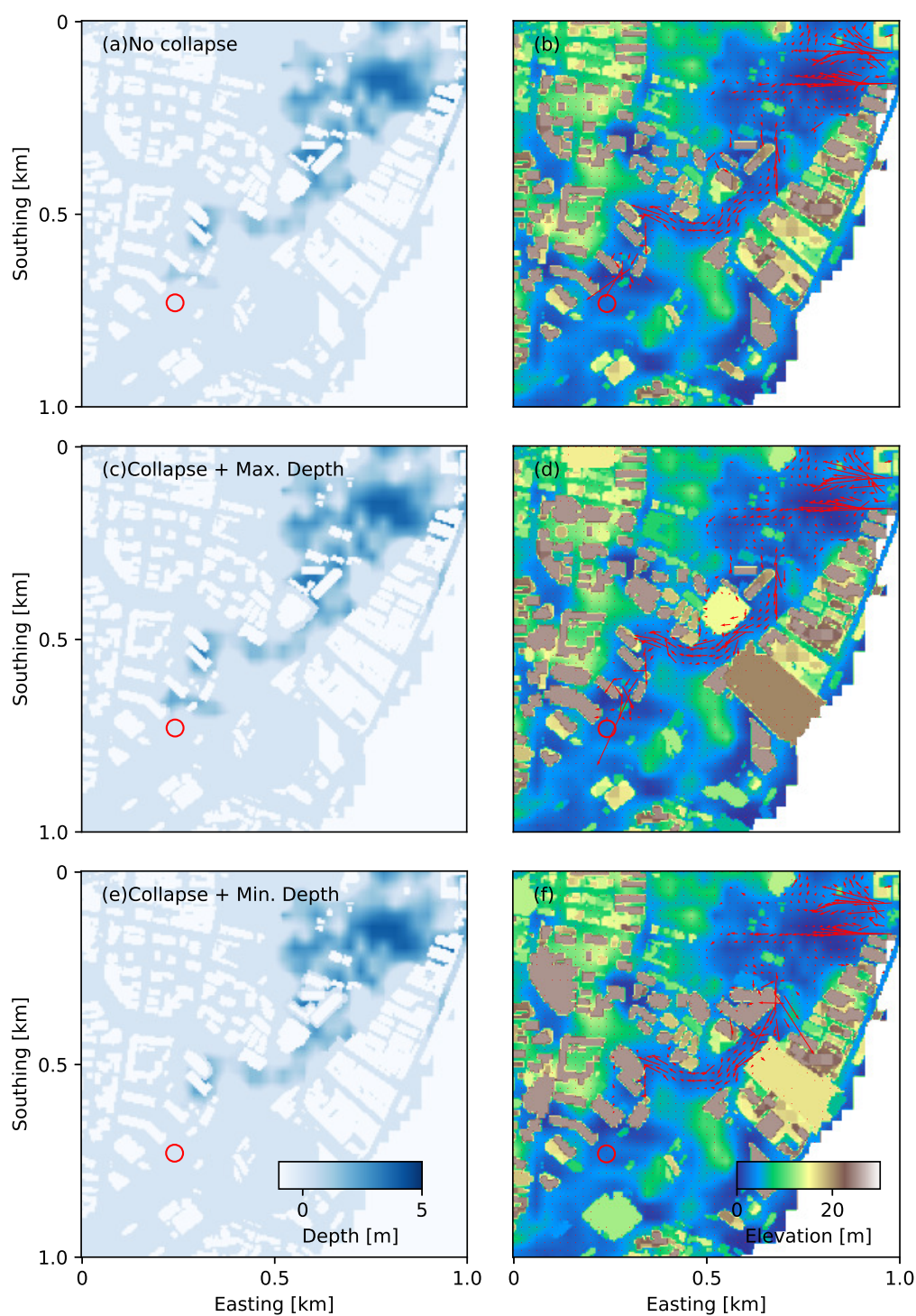
Figure 8. Simulated water depth (left column) and velocity (right column) at 2 hours for selected fluvial flood scenarios near metro station 13 (r=20%). The top row is the reference scenario without building collapse (the black curve in Fig. 7e). The middle row is associated with the building collapse scenario with the largest inundation depth at station 13, whereas the bottom row represents the scenario with the smallest inundation depth.

On the contrary, fluvial flood originate from point sources (i.e., the break points along the river bank), forming only a few travel paths from the source. However, since the invading river water is driven by strong pressure gradient, it travels through longer distances. The long travel path implies a greater probability for the flow to be interfered by the collapsed building, and the very few paths means that once it is interfered, the subsequent flood propagation will be dramatically influenced. Thus, a large r does not necessarily affect the inundation of a metro station, but when it does, the inundation statues of the station could be completely altered.

4.2 Global vs. Local

Hydrodynamic simulation is the predominant method for urban flood studies as it replicates and forecasts the spatiotemporal evolution of inundation depth and flow fields. This capability allows for a detailed examination of the complete flooding process at finer spatial and temporal resolutions. However, this advantage is not always fully exploited as many urban flood studies focus on the "global" flood variables and the "global" influencing factors. The former are the variables that characterize flood of the entire study area (e.g., inundation extent, flood volume, mean depth and outflow discharge), and the latter are the factors that are applied to the entire study area (e.g., rainfall intensity, building coverage, drainage capacity) (e.g. Bermúdez et al., 2018; Bruwier et al., 2020; David and Schmalz, 2020).

Buildings in megacities often exhibit strong spatial heterogeneity. Taking Shanghai as an example, historical buildings from the early 20th century, civil apartments from the post-World War II era, and some of the world's tallest skyscrapers coexist. These structures differ in age, height, construction, materials, usage, and earthquake resistance. Consequently, they are expected to react differently when subjected to seismic activity, indicating that earthquake-induced building collapse could be localized. Similarly, urban flood vulnerability is also localized. Metro stations are inherently more vulnerable than most other urban infrastructures. Thus, acknowledging that the collapse of a building at location A can hardly affect the flooding of location B that is kilometers away, this study adopts a local-to-local approach when analyzing results. For example, the water depth at each station is examined together with detailed building collapse patterns nearby. If we only look at global variables, for example, the inundation extent shown in Fig. 8(a), (c) and (e), minimal differences are visible between different scenarios.

Herein, we want to emphasize the importance of performing high-resolution flood simulations with HPC-enabled hydrodynamic models, which allows investigating key localized flood processes. This is particularly important in terms of risk assessment and mitigation because it is often the local spots (metro stations, bridge tunnels, narrow channels, etc.) that suffer the most severe flood disasters (e.g. Hénonin et al., 2015; Vermeij, 2016).

4.3 Limitations

With SERGHEI-SWE, the present study models the flooding of the central district of Shanghai under extreme rainfall and levee breaching events. Urban flood process also involves infiltration into the subsurface, and drainage through the stormwater pipes (e.g. Bermúdez et al., 2018; Cardoso et al., 2020; Hossain Anni et al., 2020; Schubert et al., 2022b). These two processes are neglected in this work due to the lack of data on the geological conditions, the water table and the pipe layout of the study area. Indeed, data scarcity is a major challenge when incorporating underground infrastructures with surface hydrodynamic

simulations. Although empirical methods are available to approximate the amount of soil infiltration and pipe drainage (e.g.
275 Bruwier et al., 2020; Xu et al., 2023), they are not applied herein because Shanghai as a coastal city features very shallow
water table (in the range of 1-2m). Under extreme flooding conditions the soil could reach saturation rapidly. The pipes could
reach their full capacity too. Figure 5 demonstrates that the maximum inundation depth of the July 21th flood ranges between
30 to 60cm among the metro stations, which is higher than the reported values in the media (around 25cm), but within a
reasonable range considering the absence of drainage pipes. We argue that the mechanism how building collapse affect flood
280 propagation, which is the focus of this work, is not sensitive to soil infiltration or pipe drainage. As part of the ongoing work,
SERGHEI-SWE is being developed to integrate a variably-saturated groundwater solver, and a stromwater drainage model.
The fully coupled surface-subsurface-pipe flow model should be able to provided a physically more complete picture of the
urban flooding process in the future.

In this work, building collapse is simplified as changes in the building geometry, and earthquake vulnerability (i.e., which
285 building will collapse during an earthquake) is assigned randomly. This method treats earthquake and building strength as
"global" variables, which is not aligned with our local-to-local strategy (Section 4.2). Indeed, more advanced approaches
inevitably require detailed information on the buildings in the study area, including the building height, age, usage, material and
so on (Xin et al., 2021). We argue that such information are not necessary for the present study because we put more attention
on the flood propagation mechanisms and processes. However, in future multi-hazard studies, these data should be obtained
290 and integrated with advanced building collapse models to provide more realistic, city-wide building collapse estimations.

In the present study, metro stations are simplified to single pixels on the DEM. However, real metro stations in Shanghai
often contain multiple exits spanning several road blocks. Consequently, the flooding status and flood resistance at each exit
could vary. Although further refining the grid resolution to resolve the local topography at each metro exit remains challenging,
a multi-scale approach might be feasible in the future. For example, based on the hydrodynamic simulation results at relatively
295 coarse grid resolutions (e.g., the 5m resolution used herein), a finer resolution simulation could be performed in a smaller
region near the metro station. This would characterize the detailed flooding processes at each exit. The multi-scale modeling
approach, coupled with a physics-based building collapse model, would enable a true local-to-local analysis and evaluation of
the multi-hazard risk posed to metro stations.

5 Conclusions

300 In this study, GPU-accelerated hydrodynamic simulation is employed to simulate pluvial and fluvial flood propagation before
and after earthquake-induced building collapse, aiming at understanding the mechanism how building collapse influences flood
inundation of urban metro stations. Taking Huangpu district in central Shanghai as the study area, the following conclusion are
drawn from the simulation results:

1. Pluvial flood

305 Pluvial flood occurs over a broad spatial extent. The travel paths of the flood water are relatively short due to the widely
distributed local topographic depressions that serve as natural drainage points. Thus, only the buildings collapsed near

the metro station can affect its inundation by interfering the relevant propagation paths of the water that flood the station. It also follows that the impact of building collapse on metro station flooding is positively correlated to the proportion of buildings that have collapsed.

310   2. Fluvial flood

Fluvial floods originate from point sources. The propagation of fluvial flood is characterized by long and consistent trajectories spreading from the source and following the topographic gradient. Building collapse only affect fluvial flood when the collapsed buildings are located close to the propagation path of the flood water. However, since these paths are generally longer than those for pluvial floods, the inundation of a metro station could be influenced by buildings

315   collapsed some distance away. Moreover, an increasing proportion of building collapse does not necessarily enhance the flood risk because there is a large probability that the collapsed buildings are situated far from the flood source or its travel path. The key factor is the spatial relationship between the flood propagation path, the location of building failures and the location of the hazard-bearing body of interest (e.g., a metro station).

This study provides novel insights into the complex compound mechanism involving earthquake-induced building collapse

320   and subsequent flooding under a multi-hazard context. While the findings contribute to advancing multi-hazard evolution process and risk analysis, it is important to acknowledge that the explicit modeling of earthquake processes and their physical impacts on individual buildings was beyond the scope of this work. Future research efforts should focus on developing comprehensive physical-process-based multi-hazard simulators capable of capturing the intricate dynamics of such compound events at a finer scale.

325   *Code and data availability.*

The SERGHEI-SWE model is an open-sourced software (Caviedes-Voullième et al., 2023). The topography, building and road layout data of the study area are all publicly available. The rainfall data is measured by the authors and is available upon request.

Author contributions.

330   ZL conceptualized the research aim and scope; ZZ prepared the data; ZL performed the numerical simulation; ZL and HL analyzed the results; ZL and HL wrote the manuscript draft; CD and SJ reviewed and edited the manuscript.

Competing interests.

The authors declare no competing interests.

References

Aoki, Y., Yoshizawa, A., and Taminato, T.: Anti-inundation Measures for Underground Stations of Tokyo Metro, Procedia Engineering, 165, 2–10, https://doi.org/10.1016/j.proeng.2016.11.730, 2016.

Balica, S. F., Wright, N. G., and Van Der Meulen, F.: A flood vulnerability index for coastal cities and its use in assessing climate change impacts, Natural Hazards, 64, 73–105, https://doi.org/10.1007/s11069-012-0234-1, 2012.

Bermúdez, M., Ntegeka, V., Wolfs, V., and Willems, P.: Development and Comparison of Two Fast Surrogate Models for Urban Pluvial Flood Simulations, Water Resources Management, 32, 2801–2815, https://doi.org/10.1007/s11269-018-1959-8, 2018.

Bruwier, M., Maravat, C., Mustafa, A., Teller, J., Pirotton, M., Erpicum, S., Archambeau, P., and Dewals, B.: Influence of urban forms on surface flow in urban pluvial flooding, Journal of Hydrology, 582, 124 493, https://doi.org/10.1016/j.jhydrol.2019.124493, 2020.

Cao, W., Zhou, Y., Güneralp, B., Li, X., Zhao, K., and Zhang, H.: Increasing global urban exposure to flooding: An analysis of long-term annual dynamics, Science of The Total Environment, 817, 153 012, https://doi.org/10.1016/j.scitotenv.2022.153012, 2022.

Cardoso, M. A., Almeida, M. C., Brito, R. S., Gomes, J. L., Beceiro, P., and Oliveira, A.: 1D / 2D Stormwater Modelling to Support Urban Flood Risk Management in Estuarine Areas: Hazard Assessment in the Dafundo Case Study, Journal of Flood Risk Management, 13, https://doi.org/10.1111/jfr3.12663, 2020.

Caviedes-Voullième, D., Morales-Hernández, M., Norman, M. R., and Özgen Xian, I.: SERGHEI (SERGHEI-SWE) v1.0: a performance-portable high-performance parallel-computing shallow-water solver for hydrology and environmental hydraulics, Geoscientific Model Development, 16, 977–1008, https://doi.org/10.5194/gmd-16-977-2023, 2023.

Cole, S. W., Xu, Y., and Burton, P. W.: Seismic hazard and risk in Shanghai and estimation of expected building damage, Soil Dynamics and Earthquake Engineering, 28, 778–794, https://doi.org/10.1016/j.soildyn.2007.10.008, 2008.

David, A. and Schmalz, B.: Flood Hazard Analysis in Small Catchments: Comparison of Hydrological and Hydrodynamic Approaches by the Use of Direct Rainfall, Journal of Flood Risk Management, 13, https://doi.org/10.1111/jfr3.12639, 2020.

Depietri, Y., Dahal, K., and McPhearson, T.: Multi-hazard risks in New York City, Natural Hazards and Earth System Sciences, 18, 3363–3381, https://doi.org/10.5194/nhess-18-3363-2018, 2018.

Forero-Ortiz, E., Martínez-Gomariz, E., and Cañas Porcuna, M.: A review of flood impact assessment approaches for underground infrastructures in urban areas: a focus on transport systems, Hydrological Sciences Journal, 65, 1943–1955, https://doi.org/10.1080/02626667.2020.1784424, 2020.

Gautam, D. and Dong, Y.: Multi-hazard vulnerability of structures and lifelines due to the 2015 Gorkha earthquake and 2017 central Nepal flash flood, Journal of Building Engineering, 17, 196–201, https://doi.org/10.1016/j.jobe.2018.02.016, 2018.

Gill, J. C. and Malamud, B. D.: Reviewing and visualizing the interactions of natural hazards: Interactions of Natural Hazards, Reviews of Geophysics, 52, 680–722, https://doi.org/10.1002/2013RG000445, 2014.

Goda, K., Mori, N., Yasuda, T., Prasetyo, A., Muhammad, A., and Tsujio, D.: Cascading Geological Hazards and Risks of the 2018 Sulawesi Indonesia Earthquake and Sensitivity Analysis of Tsunami Inundation Simulations, Frontiers in Earth Science, 7, 261, https://doi.org/10.3389/feart.2019.00261, 2019.

Guinot, V., Delenne, C., Rousseau, A., and Boutron, O.: Flux Closures and Source Term Models for Shallow Water Models with Depth-Dependent Integral Porosity, Advances in Water Resources, 122, 1–26, https://doi.org/10.1016/j.advwatres.2018.09.014, 2018.

Guo, K., Guan, M., and Yu, D.: Urban surface water flood modelling – a comprehensive review of current models and future challenges, Hydrology and Earth System Sciences, 25, 2843–2860, https://doi.org/10.5194/hess-25-2843-2021, 2021.

Hodges, B. R.: Representing Hydrodynamically Important Blocking Features in Coastal or Riverine Lidar Topography, Natural Hazards and Earth System Sciences, 15, 1011–1023, https://doi.org/10.5194/nhess-15-1011-2015, 2015.

375 Hossain Anni, A., Cohen, S., and Praskievicz, S.: Sensitivity of Urban Flood Simulations to Stormwater Infrastructure and Soil Infiltration, Journal of Hydrology, 588, 125 028, https://doi.org/10.1016/j.jhydrol.2020.125028, 2020.

Hénonin, J., Ma, H., Yang, Z.-Y., Hartnack, J., Havnø, K., Gourbesville, P., and Mark, O.: Citywide multi-grid urban flood modelling: the July 2012 flood in Beijing, Urban Water Journal, 12, 52–66, https://doi.org/10.1080/1573062X.2013.851710, 2015.

Ito, E., Kawase, H., Matsushima, S., and Hatayama, M.: Tsunami evacuation simulation considering road blockage by collapsed buildings

380 evaluated from predicted strong ground motion, Natural Hazards, 101, 959–980, https://doi.org/10.1007/s11069-020-03903-2, 2020.

Johnston, J., Cassalho, F., and Miesse, T.: Projecting the effects of land subsidence and sea level rise on storm surge flooding in Coastal North Carolina, Scientific Reports, 11, 21 679, https://doi.org/10.1038/s41598-021-01096-7, 2021.

Ke, Q., Yin, J., Bricker, J. D., Savage, N., Buonomo, E., Ye, Q., Visser, P., Dong, G., Wang, S., Tian, Z., Sun, L., Toumi, R., and Jonkman, S. N.: An integrated framework of coastal flood modelling under the failures of sea dikes: a case study in Shanghai, Natural Hazards, 109,

385 671–703, https://doi.org/10.1007/s11069-021-04853-z, 2021.

Li, Z. and Hodges, B. R.: Modeling Subgrid-Scale Topographic Effects on Shallow Marsh Hydrodynamics and Salinity Transport, Advances in Water Resources, 129, 1–15, https://doi.org/10.1016/j.advwatres.2019.05.004, 2019.

Lyu, H.-M., Shen, S.-L., Zhou, A., and Yang, J.: Perspectives for flood risk assessment and management for mega-city metro system, Tunnelling and Underground Space Technology, 84, 31–44, https://doi.org/10.1016/j.tust.2018.10.019, 2019.

390 Lyu, H.-M., Zhou, W.-H., Shen, S.-L., and Zhou, A.-N.: Inundation risk assessment of metro system using AHP and TFN-AHP in Shenzhen, Sustainable Cities and Society, 56, 102 103, https://doi.org/10.1016/j.scs.2020.102103, 2020.

Morales-Hernández, M., Sharif, M. B., Kalyanapu, A., Ghafoor, S., Dullo, T., Gangrade, S., Kao, S.-C., Norman, M., and Evans, K.: TRITON: A Multi-GPU open source 2D hydrodynamic flood model, Environmental Modelling & Software, 141, 105 034, https://doi.org/10.1016/j.envsoft.2021.105034, 2021.

395 Navarro-Hernandez, M., Valdes-Abellan, J., Tomas, R., Tessitore, S., Ezquerro, P., and Herrera, G.: Analysing the Impact of Land Subsidence on the Flooding Risk: Evaluation Through InSAR and Modelling, Water Resources Management, 37, 4363–4383, https://doi.org/10.1007/s11269-023-03561-6, 2023.

Owolabi, T. A. and Sajjad, M.: A global outlook on multi-hazard risk analysis: A systematic and scientometric review, International Journal of Disaster Risk Reduction, 92, 103 727, https://doi.org/10.1016/j.ijdrr.2023.103727, 2023.

400 Rentschler, J., Avner, P., Marconcini, M., Su, R., Strano, E., Vousdoukas, M., and Hallegatte, S.: Global evidence of rapid urban growth in flood zones since 1985, Nature, 622, 87–92, https://doi.org/10.1038/s41586-023-06468-9, 2023.

Román-de La Sancha, A., Silva, R., Areu-Rangel, O. S., Verduzco-Zapata, M. G., Mendoza, E., López-Acosta, N. P., Ossa, A., and García, S.: Modelling the sequential earthquake–tsunami response of coastal road embankment infrastructure, Natural Hazards and Earth System Sciences, 22, 2589–2609, https://doi.org/10.5194/nhess-22-2589-2022, 2022.

405 Sanders, B. F. and Schubert, J. E.: PRIMo: Parallel raster inundation model, Advances in Water Resources, 126, 79–95, https://doi.org/10.1016/j.advwatres.2019.02.007, 2019.

Schubert, J. E., Luke, A., AghaKouchak, A., and Sanders, B. F.: A Framework for Mechanistic Flood Inundation Forecasting at the Metropolitan Scale, Water Resources Research, 58, e2021WR031 279, https://doi.org/10.1029/2021WR031279, 2022a.

Schubert, J. E., Luke, A., AghaKouchak, A., and Sanders, B. F.: A Framework for Mechanistic Flood Inundation Forecasting at the Metropoli-

410 tan Scale, Water Resources Research, 58, e2021WR031 279, https://doi.org/10.1029/2021WR031279, 2022b.

Takabatake, T., Chenxi, D. H., Esteban, M., and Shibayama, T.: Influence of road blockage on tsunami evacuation: A comparative study of three different coastal cities in Japan, International Journal of Disaster Risk Reduction, 68, 102 684, https://doi.org/10.1016/j.ijdrr.2021.102684, 2022.

Toda, K., Kawaike, K., Yoneyama, N., Fukakusa, S., and Yamamoto, D.: Underground Inundation Analysis by Integrated Urban Flood Model, p. 166–171, Springer Berlin Heidelberg, Berlin, Heidelberg, ISBN 978-3-540-89464-3, https://doi.org/10.1007/978-3-540-89465-0_31, 2009.

Trott, C. R., Lebrun-Grandié, D., Arndt, D., Ciesko, J., Dang, V., Ellingwood, N., Gayatri, R., Harvey, E., Hollman, D. S., Ibanez, D., Liber, N., Madsen, J., Miles, J., Poliakoff, D., Powell, A., Rajamanickam, S., Simberg, M., Sunderland, D., Turcksin, B., and Wilke, J.: Kokkos 3: Programming Model Extensions for the Exascale Era, IEEE Transactions on Parallel and Distributed Systems, 33, 805–817, https://doi.org/10.1109/TPDS.2021.3097283, 2022.

Vermeij, D.: Flood risk reduction interventions for the New York City subway system: A research on the impact of storm surge and sea level rise on the safety against flooding in urban delta's, Master's Thesis, TU Delft, 2016.

Wang, G., Liu, Y., Hu, Z., Zhang, G., Liu, J., Lyu, Y., Gu, Y., Huang, X., Zhang, Q., and Liu, L.: Flood Risk Assessment of Subway Systems in Metropolitan Areas under Land Subsidence Scenario: A Case Study of Beijing, Remote Sensing, 13, 637, https://doi.org/10.3390/rs13040637, 2021.

Wilfong, M., Patra, D., Pavao-Zuckerman, M., and Leisnham, P. T.: Diffusing responsibility, decentralizing infrastructure: hydrosocial relationships within the shifting stormwater management paradigm, Journal of Environmental Planning and Management, 67, 830–851, https://doi.org/10.1080/09640568.2022.2133687, 2024.

Xin, D., Daniell, J. E., Tsang, H.-H., and Wenzel, F.: Residential Building Stock Modelling for Mainland China Targeted for Seismic Risk Assessment, Natural Hazards and Earth System Sciences, 21(10), 3031–3056, https://doi.org/10.5194/nhess-21-3031-2021, 2021.

Xu, K., Fang, J., Fang, Y., Sun, Q., Wu, C., and Liu, M.: The Importance of Digital Elevation Model Selection in Flood Simulation and a Proposed Method to Reduce DEM Errors: A Case Study in Shanghai, International Journal of Disaster Risk Science, 12, 890–902, https://doi.org/10.1007/s13753-021-00377-z, 2021.

Xu, S., Chen, Y., Zhang, Y., Chen, L., Sun, H., and Liu, J.: Developing a Framework for Urban Flood Modeling in Data-poor Regions, Journal of Hydrology, 617, 128 985, https://doi.org/10.1016/j.jhydrol.2022.128985, 2023.

Yang, H., Zhao, L., and Chen, J.: Metro System Inundation in Zhengzhou, Henan Province, China, Sustainability, 14, 9292, https://doi.org/10.3390/su14159292, 2022.

Yin, J., Lin, N., Yang, Y., Pringle, W. J., Tan, J., Westerink, J. J., and Yu, D.: Hazard Assessment for Typhoon-Induced Coastal Flooding and Inundation in Shanghai, China, Journal of Geophysical Research: Oceans, 126, e2021JC017 319, https://doi.org/10.1029/2021JC017319, 2021.

Zhou, Z., Liu, S., Zhong, G., and Cai, Y.: Flood Disaster and Flood Control Measurements in Shanghai, Natural Hazards Review, 18, B5016 001, https://doi.org/10.1061/(ASCE)NH.1527-6996.0000213, 2017.